16

Stability Analysis of Underground Caverns Based on the Unified Strength Theory

16.1 Introduction

In recent years, there has been an increasing interest internationally in the construction of large-scale underground powerhouses. The stability analysis of underground caverns in a hydropower station is often related to the safe operation of the whole station and provides enormous benefits. Due to their large scale, complicated space configurations and reactions between caverns, stability analysis of underground powerhouses is a very difficult and challenging task. Hence, the accurate description of the mechanical behavior of the rock mass and the selection of the rock properties is a very important research topic in underground construction.

The stability of large caverns has been investigated widely. To explore some aspects of the complex geometrical shape, the stress boundary conditions obtained from in-situ stress measurement and constitutive models for the rock mass, large caverns have been studied by Professor Qiao and Li Y. Based on the engineering background of Huanren pumped-storage powerhouse, the unified strength theory as a failure criterion was used in their study to analyze the stability of the main powerhouse and transformer cave and to carry out an investigation of underground excavation and support. The effect of the intermediate principal stress on rock failure and the support design will be discussed in this chapter.

This chapter is contributed by Professors Li Y and Qiao L, Beijing Science and Technical University, Beijing, China

M.-H. Yu et al., *Computational Plasticity*

16.2 Huanren Pumped-Storage Powerhouse and Geology

Huanren underground pumped-storage powerhouse is located in Tongtiangou, which is 4 km away from Huanren County, Liaoning Province, China. The project plans to utilize Huanren reservoir as the lower storage reservoir and to construct a dam in Tongtiangou gulley as the upper reservoir. A diversion tunnel is to connect with the underground powerhouse. The pivotal engineering construction mainly consists of the main dam, auxiliary dam of the upper reservoir, diversion tunnel and underground powerhouse. The maximum height of the main dam is 106 m and the length of the dam top is 632 m. The height of the auxiliary dam is 15 m and the length is 403.33 m. The underground powerhouse is located in the middle of the diversion tunnel and is 22.3 m wide, 50 m high and 136.2 m long.

The engineering region is covered with mountains and gullies. The mountain heights are all about 500~700 m and a few of them are over 1000 m high. The volcanic rocks formed in the Jurassic period of the Mesozoic era are widely distributed in the station area and are shaped into cuestas, mesas and all kinds of valleys.

16.2.1 The Powerhouse Region

The powerhouse zone is 136 m long, 22 m wide, 50 m high and 230 m deep. It is located in the interbeds of andesite-tuff and tuff-agglomerate with some tuff-agglomerate rocks near the top. And the direction angle of the axes is NE 15°. The RQD value of the zone is 95%, the acoustic velocity for andesite-tuff is 5.06 km/s, the acoustic velocity for the interbeds is 3.41~5.05 km/s and the associated integrity coefficients are 0.95 and 0.43~0.99.

The rock masses are almost intact, but the lithology of the 16th bed is complicated. In this bed, there are about ten strata of andesite-tuff which are 0.5~5 m thick and show poor properties. The strata will crack and fail when losing water, and have bad stability as well. There is a band standing at a borehole depth of 263 m (elevation of 267 m). The band with bad geological conditions is 15 cm thick, made up of green clay and rock fragments. The angle, measured in the axis of powerhouse tunnel from the band's strike direction, is only 15°~25°, and inclines toward the tunnel. It is very unfavorable for the stabilization of downstream sidewalls. The 15th layer of the tuff rock which is 3 m away from the tunnel's roof causes harm to the stability. In addition, a set of joints which strike NNE is dangerous for sidewall stability too.

16.2.2 In Situ Stress Measurement in Huanren Pumped Storage Powerhouse

The in-situ stress measurement involved in this project includes seven measurement sites. The figures obtained during the tests showed the same results.

According to the data obtained by the strain collector, stresses were calculated. An average was introduced when measurements were taken more than two times at one site. The gauge has 12 separate strain gauges, in rosettes of three, and there was some redundancy in the measurements. Thus statistical analysis of the least square method has been made.

16.3 Comparison of Failure Criteria for Geomaterials

Failure criteria can be used to understand the materials' response to loads, to determine the failure conditions in different stress states. The selection of failure criteria has a great impact on calculating the results of geotechnical engineering. Because of the differences between geomaterials and general materials in constitutive behavior, it is necessary to choose a suitable yield or failure criterion in engineering applications for purposes of economy and safety.

Various strength criteria have been developed in the past to describe the behavior of rock masses. Of these, the linear Mohr-Coulomb criterion and the nonlinear Hoek-Brown strength criterion are two of the most widely used strength criteria in geotechnical engineering. The Mohr-Coulomb failure criterion can be expressed as

$$\tau_f = c + \sigma \cdot \tan\phi \tag{16.1}$$

where ι_f is the shear strength, c is the cohesion, ϕ is the friction angle and σ is the normal stress at the shear plane.

Currently, the Mohr-Coulomb strength theory is widely used. It explains that the tensile strength of rocks is much smaller than their shear strength. In addition, a specimen will yield under triaxial constant tension loading conditions and will not fail under triaxial constant compression loading conditions. The Mohr-Coulomb strength theory, however, only considers the effects of two principal stresses σ_1 and σ_3, but ignores the influence of σ_2. Mogi (1967; 1979) and Xu et al. (1985; 1986) and Li and Xu (1990) have proved the effects of σ_2 by using true tri-axial tests. Hence, the Mohr-Coulomb strength theory is an imperfect strength criterion.

The Drucker-Prager criterion is an extension of the Huber von Mises criterion, and is a modification of the Huber-von Mises yield criterion by adding a hydrostatic stress term. Zhu-Jiang Shen calls it a three-shear yield criterion. The expression is

$$F = F(I_1, J_2) = \sqrt{J_2} - \alpha I_1 = k \tag{16.2}$$

or

$$F = F(p, q) = q - 3\sqrt{3}\alpha p = \sqrt{3}k \tag{16.3}$$

where α and k are material parameters which can be deduced from the cohesion and the internal angle of friction.

The intermediate principal stress and the hydrostatic stress are taken into account in the Drucker-Prager criterion. The criterion has been widely used and popularized after it was proposed. However, under some conditions, the criterion contradicts the experimental results. Hence, the criterion has seldom been used in recent years.

The Hoek-Brown failure criterion is an empirical criterion which is derived from experimental data obtained from some triaxial compression tests performed on rocks. Since its first introduction, the criterion has been modified several times. For a jointed rock, the Hoek-Brown failure criterion has been found more suitable than the Mohr-Coulomb criterion. The Hoek-Brown strength parameters can be estimated based on the GSI system, which provides the guidance for the peak strength estimation of rock masses. The latest version of the generalized Hoek-Brown criterion for jointed rock masses is defined by

$$\sigma_1 = \sigma_3 + \sigma_{ci}(m_b \frac{\sigma_3}{\sigma_{ci}} + s)^a \tag{16.4}$$

where σ_3 and σ_{ci} are the minimum principal stress and the uniaxial compressive strength (UCS) of the intact rock, respectively, m_b, s and a are rock mass strength parameters which depend upon the characteristics of the rock mass. The parameters can be determined by using the GSI index and m_i value.

The effect of intermediate principal stress, however, is not taken into account both in the Mohr-Coulomb and the Hoek-Brown strength criteria. Maohong Yu demonstrates that the maximum principal shear stress τ_{13} is always equal to the sum of the other two principal shear stresses τ_{12} and τ_{23}, i.e., $\tau_{13}=\tau_{12}+\tau_{23}$, which means that there are only two independent components in three principal shear stresses. So failure criteria consider the effects of the two relatively larger principal shear stresses. According to the change in the intermediate principal stress, Yu proposed mathematical modeling in the form of twin formulas. Based on the twin-shear criterion (Yu, 1961a; 1985), a parameter related to the effect of intermediate principal stress is considered. The unified strength theory assumes that the materials start to yield when the sum of the two larger principal shear stresses and the corresponding normal stress function reaches a constant value. The mathematical modeling can be expressed as follows:

$$F = \tau_{13} - \beta\sigma_{13} + b(\tau_{12} - \beta\sigma_{12}) = K \quad (\tau_{12} - \beta\sigma_{12} \geq \tau_{23} - \beta\sigma_{23}) \tag{16.5}$$

$$F' = \tau_{13} - \beta\sigma_{13} + b(\tau_{23} - \beta\sigma_{23}) = K \quad (\tau_{12} - \beta\sigma_{12} \leq \tau_{23} - \beta\sigma_{23}) \tag{16.6}$$

where b is a parameter reflecting the influence of the intermediate principal shear stress on the yield of materials. In terms of the convex failure criteria, the value of b ranges from 0 to 1. β is the coefficient representing the effect of the normal stress on the yield and K is a strength parameter of the material. β and K can be expressed as

$$\beta = \frac{1-\alpha}{1+\alpha}, \quad K = \frac{2}{1+\alpha}\sigma_t, \quad \alpha = \frac{\sigma_t}{\sigma_c} \tag{16.7}$$

The shear stresses $\tau_{13}, \tau_{12}, \tau_{23}$ and normal stresses $\sigma_{13}, \sigma_{12}, \sigma_{23}$ can be written by

$$\tau_{13} = \frac{1}{2}(\sigma_1 - \sigma_3),\ \tau_{12} = \frac{1}{2}(\sigma_1 - \sigma_2),\ \tau_{23} = \frac{1}{2}(\sigma_2 - \sigma_3) \tag{16.8}$$

$$\sigma_{13} = \frac{1}{2}(\sigma_1 + \sigma_3),\ \sigma_{23} = \frac{1}{2}(\sigma_2 + \sigma_3),\ \sigma_{12} = \frac{1}{2}(\sigma_1 + \sigma_2) \tag{16.9}$$

The unified strength theory can be used in yield analysis for a wide range of materials, and each proposed strength criterion is just a special type of the unified strength criterion. The unified strength theory consists of twin functions and corresponding limited conditions. The suitable formula should be chosen according to the stress state when the criterion is used. The same strength of materials can be obtained when the two limited conditions are both satisfied simultaneously.

16.4 Determination of Rock Mass Strength Parameters

The effect of intermediate principal stress is not considered in the Mohr-Coulomb and the Hoek-Brown strength criteria, which means that the two strength criteria cannot reasonably reflect the characteristics of variability in rock strength when the intermediate principal stress changes. The unified strength theory incorporates the intermediate principal stress and can choose different parameters according to the data resulting from true triaxial tests on rocks or rock masses. The unified strength theory cannot solve the problem of the yield angle, but this will not affect the deduction of the flow rule used for continuum modeling. The unified yield criterion does not contradict the other strength criteria, while the other criteria are the special cases of the unified strength criterion.

In this study, the unified strength theory is chosen as the failure criterion for the stability analysis of Huanren pumped-storage powerhouse, and the Hoek-Brown criterion is chosen for the determination of parameters from the test data.

For good-quality andesite, Hoek-Brown strength parameters m_b, s and α are estimated to be 1.7, 0.004 and 0.5, respectively, and the uniaxial compressive strength of the intact rock is 70 MPa. Considering the parameters, the criterion can be expressed as

$$F = \sigma_1 - \sigma_3 - \sqrt{1.7 \times 70\sigma_3 + 0.004 \times 70^2} = 0 \tag{16.10}$$

It is deduced from Eq. (16.10) that σ_1 is equal to 68.9 MPa when the compressive strength of the rock mass is 4.43 MPa and σ_3=20 MPa. After substituting the parameters mentioned above in Eq. (16.5), we obtain $\beta = 0.53$, $\frac{K}{1+b} = 1.034$. Thus $\alpha = 0.31$ can be calculated from Eq. (16.7) and $\sigma_t = \sigma_c \cdot \alpha = 1.36$ MPa from Eq. (16.7). The parameter b will be determined by the experimental results of true tri-axial tests.

16.5 Constitutive Formulation of Unified Strength Theory Used for Fast Lagrangian Analysis

Incremental formulations similar to those of the Mohr-Coulomb model in Flac-3D are used, i.e., only the elastic part of the strain increment will contribute to the stress increment and the elastic behavior is linear. The equations have the forms

$$\Delta\sigma_1 = \alpha_1 \Delta\varepsilon_1^e + \alpha_2 (\Delta\varepsilon_2^e + \Delta\varepsilon_3^e) \tag{16.11}$$

$$\Delta\sigma_2 = \alpha_1 \Delta\varepsilon_2^e + \alpha_2 (\Delta\varepsilon_1^e + \Delta\varepsilon_3^e) \tag{16.12}$$

$$\Delta\sigma_3 = \alpha_1 \Delta\varepsilon_3^e + \alpha_2 (\Delta\varepsilon_1^e + \Delta\varepsilon_2^e) \tag{16.13}$$

where α_1 and α_2 are material constants defined by the shear modulus G, and bulk modulus.

$$\alpha_1 = K + \frac{4}{3}G \tag{16.14}$$

$$\alpha_2 = K - \frac{2}{3}G \tag{16.15}$$

The unified form from Eq. (16.11) to Eq. (16.13) can be expressed as

$$\Delta\sigma_i = S_i(\Delta\varepsilon_n^e), \quad (i=1, n) \tag{16.16}$$

The failure criterion can be written as

$$f\left(\sigma_n\right)=0 \tag{16.17}$$

where f is the yield function based on the unified strength theory. The strain increment can be decomposed into elastic and plastic components from the following equation.

$$\Delta\varepsilon_i=\Delta\varepsilon_i^e+\varepsilon_i^p \tag{16.18}$$

The new stress-vector components must comply with the yield function, which can be expressed as

$$f(\sigma_n+\Delta\sigma_n)=0 \tag{16.19}$$

A non-associated shear plastic flow rule and an associated tensile plastic flow rule are defined in the Flac-3D model. But the tensile failure is a special case of shear failure according to the unified strength theory, so only a non-associated shear plastic flow rule is used. The form is given by

$$\Delta\varepsilon_i^p=\lambda\frac{\partial g}{\partial\sigma_i} \tag{16.20}$$

From the further expression of the plastic strain increment in the flow rule, the stress increment can be written as

$$\Delta\sigma_i=S_i(\Delta\varepsilon_n)-\lambda S_i\left(\frac{\partial g}{\partial\sigma_n}\right) \tag{16.21}$$

where $S_i\left(\Delta\varepsilon_n\right)$ is linear. The strength criterion is a linear function of principal stresses, so Eq.(16.19) is expressed as

$$f\left(\sigma_n\right)+f^*\left(\Delta\sigma_n\right)=0 \tag{16.22}$$

where f^* represents the function f minus its constant term. For a stress point σ_n on the yield surface, there is $f\left(\sigma_n\right)$=0. After considering Eq. (16.21) for the stress increment in Eq. (16.22), there is

$$f^*\left[S_n\left(\Delta\varepsilon_n\right)\right]-\lambda f^*\left[S_n\left(\frac{\partial g}{\partial\sigma_n}\right)\right]=0 \tag{16.23}$$

The new total stress increment σ_i^N and elastic guesses σ_i^I can be expressed

as follows:

$$\sigma_i^N = \sigma_i + \Delta\sigma_i \tag{16.24}$$

$$\sigma_i^I = \sigma_i + S_i(\Delta\varepsilon_n) \tag{16.25}$$

Using the same method as above, Eq. (16.25) can be written as

$$f\left(\sigma_n^I\right) = f^*\left[S_n(\Delta\varepsilon_n)\right] \tag{16.26}$$

It can be derived from Eqs. (16.23) and (16.26) that

$$\lambda = \frac{f\left(\sigma_n^I\right)}{f^*\left[S_n\left(\dfrac{\partial g}{\partial \sigma_n}\right)\right]} \tag{16.27}$$

From Eqs. (16.21), (16.24), (16.25) and (16.27), we can obtain

$$\sigma_i^N = \sigma_i^I - \lambda S_i\left(\frac{\partial g}{\partial \sigma_n}\right) \tag{16.28}$$

Unlike metal materials, geomaterials comply with non-associated flow rules. But, so far, the non-associated flow rules have not been clearly proposed. Taking the definition of unified strength theory and the general principles of Flac-3D into consideration, a special non-associated flow rule is discussed in this case.

First, if the associated flow rule is applied, just as for the arguments used in traditional plastic mechanics, the rule can be expressed as follows:

(i) When $\tau_{12} + \beta\sigma_{12} \geq \tau_{23} + \beta_{23}$ (Take tensile stress as positive)

$$\frac{\partial g}{\partial \sigma_1} = -1 \tag{16.29}$$

$$\frac{\partial g}{\partial \sigma_2} = \frac{\alpha b}{1+b} \tag{16.30}$$

$$\frac{\partial g}{\partial \sigma_3} = \frac{\alpha}{1+b} \tag{16.31}$$

(ii) When $\tau_{12} + \beta\sigma_{12} \leq \tau_{23} + \beta_{23}$ (Take tensile stress as positive)

$$\frac{\partial g}{\partial \sigma_1} = -\frac{1}{1+b} \tag{16.32}$$

$$\frac{\partial g}{\partial \sigma_2} = -\frac{b}{1+b} \tag{16.33}$$

$$\frac{\partial g}{\partial \sigma_3} = \alpha \tag{16.34}$$

Then we can incorporate the flow rule into the modeling of Flac-3D. We find that the rock dilation is too large zones in the failure model. So a non-associated flow rule should be used here.

The flow rules used in Flac-3D derive from the associated flow rules by modifying some parameters, e.g., the forms of the Mohr-Coulomb strength theory and Drucker-Prager criterion. And, traditionally, the dilation angle is used for the evaluation of the plastic expansion of rock. So the equations are modified corresponding to the non-associated law as follows:

(i) When $\tau_{12} + \beta\sigma_{12} \geq \tau_{23} + \beta_{23}$ (Take tensile stress as positive)

$$\frac{\partial g}{\partial \sigma_1} = -1 \tag{16.35}$$

$$\frac{\partial g}{\partial \sigma_2} = \frac{\alpha' b}{1+b} \tag{16.36}$$

$$\frac{\partial g}{\partial \sigma_3} = \frac{\alpha'}{1+b} \tag{16.37}$$

(ii) When $\tau_{12} + \beta\sigma_{12} \leq \tau_{23} + \beta_{23}$ (Take tensile stress as positive)

$$\frac{\partial g}{\partial \sigma_1} = -\frac{1}{1+b} \tag{16.38}$$

$$\frac{\partial g}{\partial \sigma_2} = -\frac{b}{1+b} \tag{16.39}$$

$$\frac{\partial g}{\partial \sigma_3} = \alpha' \tag{16.40}$$

where $\alpha' = \dfrac{1-\sin(\psi)}{1+\sin(\psi)}$, and ψ is the dilation angle of the rock.

Taking the compressive stress as positive, and changing the coefficient of the first principal stress to a constant, we obtain the following:

(i) When $\tau_{12} - \beta\sigma_{12} \geq \tau_{23} - \beta_{23}$ (Take compressive stress as positive)

$$\frac{\partial g}{\partial \sigma_1} = 1 \tag{16.41}$$

$$\frac{\partial g}{\partial \sigma_2} = b \tag{16.42}$$

$$\frac{\partial g}{\partial \sigma_3} = -N_\psi \left(1 + b\right) \tag{16.43}$$

(ii) When $\tau_{12} - \beta\sigma_{12} \le \tau_{23} - \beta_{23}$ (Take compressive stress as positive)

$$\frac{\partial g}{\partial \sigma_1} = 1 \tag{16.44}$$

$$\frac{\partial g}{\partial \sigma_2} = -N_\psi \frac{b}{1+b} \tag{16.45}$$

$$\frac{\partial g}{\partial \sigma_3} = -N_\psi \frac{1}{1+b} \tag{16.46}$$

when b=0, the Mohr-Coulomb strength theory can be deduced from the unified strength theory and the expressions from Eq. (16.41) to Eq. (16.46) have the same forms of the Mohr-Coulomb flow rule used in Flac-3D. According to the equations from Eq. (16.41) to Eq. (16.46), we have

$$\frac{\partial g}{\partial \sigma_1} = 1 \tag{16.47}$$

$$\frac{\partial g}{\partial \sigma_2} = 0 \tag{16.48}$$

$$\frac{\partial g}{\partial \sigma_3} = -N_\psi \tag{16.49}$$

The advantages of the flow rule used here are as follows:

(a) In common with the Mohr-Coulomb theory, a dilation angle is incorporated into functions to account for rock dilation, which is caused by the creation and propagation of cracks during rock deformation. The value of the dilation angle can be zero when the dilation needs not to be considered.

(b) Taking the effect of the intermediate principal stress into account, relationships have been perfectly established between the unified strength theory and the Flac-3D numerical modeling. (e.g. if some parameters are used in the unified strength theory for the deduction of the Mohr-Coulomb strength criterion, by choosing the same parameters in the unified strength model defined in Flac-3D, we will get the same equations for the flow rule as Mohr-Coulomb's criterion used in Flac-3D.)

When strain-hardening or strain-softening does not take place, the relationships between stresses and the criterion can be expressed as

$$F(\sigma_i) = 0,\ \mathrm{d}F = \frac{\partial F}{\partial \sigma_i}\mathrm{d}\sigma_i < 0 \qquad \text{(Unloading conditions);}$$

$$F(\sigma_i) = 0,\ \mathrm{d}F = \frac{\partial F}{\partial \sigma_i}\mathrm{d}\sigma_i = 0 \qquad \text{(Loading conditions);}$$

$$F(\sigma_i) < 0 \qquad \text{(Elastic state).}$$

16.6 Development of Unified Strength Theory Model in Flac-3D

The methodology of writing new constitutive models in Flac-3D is called UDM (User-defined Model). The model must be developed in the C++ language and complied as a DLL file In order to create a new constitutive model, the following header files are necessary:

(a) AXES.H — specifies a particular axes system;

(b) CONMODEL.H — utility structure used to communicate with constitutive model;

(c) CONTABLE.H — defines the TABLE interface for general constitutive models;

(d) STENSOR.H— symmetric tensor storage.

Users only need to program the personal header file and classes.

(a) USERMODEL. H— user-defined head file;

(b) USERMODEL. CPP— listing of member functions.

After creating a workspace in VC++, we can create a user-defined DLL module, which contains the six files mentioned above. Before the UDM model is developed in Flac-3D, USERMODEL.DLL must be registered and loaded.

In this case, the model's name is "Double-Shear"(Twin-Shear), and the essentially parameters are bulk modulus (bulk), shear modulus (shear), dilation angle (dilation), the parameter b (bxi), the parameter α (afa) and uniaxial tensile strength (tension). In addition, the contours of the elastic modulus and Poisson's ratio can be plotted out as zones. Hence, the user-defined model can be associated and implemented in the same ways as other basic constitutive models provided in Flac-3D.

16.7 Test of User-Defined Unified Strength Theory Constitutive Model in Flac-3D

As shown in Fig. 16.1, the model is 50 mm long, 50 mm wide and 100 mm

high. First, fixing z-velocities of the top and bottom surfaces and applying 100 MPa confining pressure, we obtain a balance of the elastic model. The property parameters are listed in Table 16.1. Thereafter, the Mohr-Coulomb model is associated with the zones and the velocity is applied on the top surface in thenegative direction of the z-axis instead to the foregoing constraint of the surface. A history command is adopted to monitor the variations in the displacement and stresses. The stress-strain curves for different parameters are shown in Fig. 16.2 for the rock compression process.

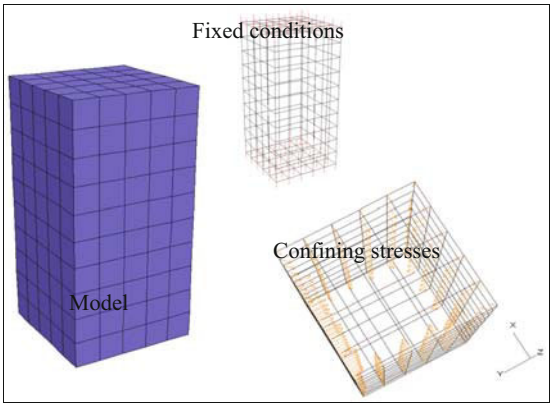

Fig. 16.1 Model zones and boundary conditions.

Table 16.1 Mohr-Coulomb strength parameters in the first simulation test

Input parameters	Values
$\sigma_2(\sigma_x)$	100 (Mpa)
$\sigma_3(\sigma_y)$	100 (MPa)
c	1 (MPa)
φ	10 (°)
Bulk	200 (MPa)
Shear	200 (MPa)

Table 16.2 Mohr-Coulomb strength parameters in the second simulation test

Input parameters	Values
$\sigma_2(\sigma_x)$	110 (Mpa)
$\sigma_3(\sigma_y)$	100 (MPa)
C	1 (MPa)
φ	10 (°)
Bulk	200 (MPa)
Shear	200 (MPa)

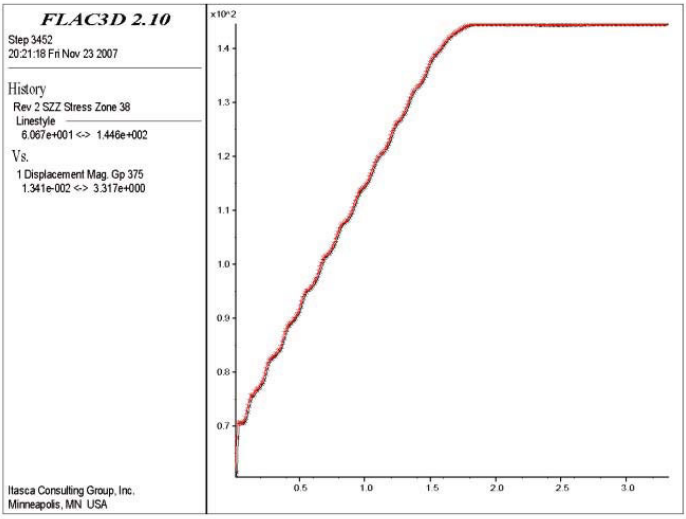

Fig. 16.2 Stress-strain curves of the two Mohr-Coulomb models with different parameters

Under the same stresses and boundary conditions, the unified strength model is used for comparison. The input parameters are shown in Table 16.3. A series of b values with b=0, b=0.5, b=0.8, and b=1 are inputted into the model in sequence and the final results can be found, as shown in Fig. 16.3.

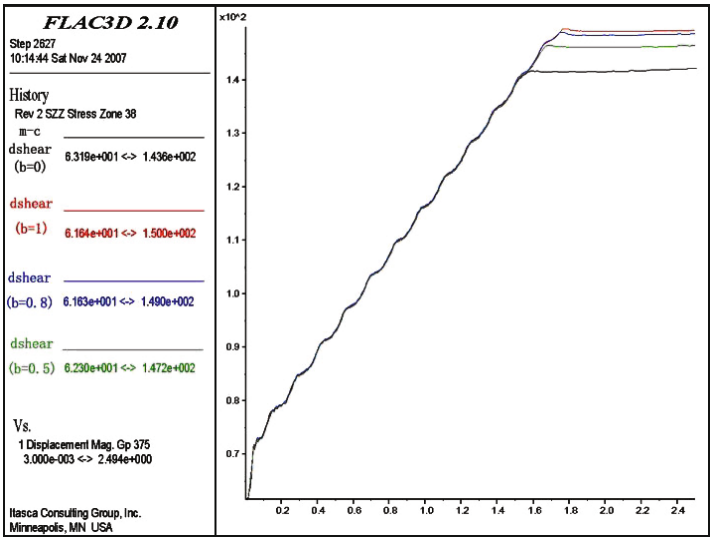

Fig. 16.3 Stress-strain curves of unified strength model with different values of b

Table 16.3 Parameters of the model associated with the unified strength theory

Input parameters	Values
$\sigma_2(\sigma_x)$	110 (MPa)
$\sigma_3(\sigma_y)$	100 (MPa)
Tensile stress	1.68 (MPa)
α	0.71 (º)
Bulk	200 (MPa)
Shear	200 (MPa)

It can be seen that the result is the same with the curve of the Mohr-Coulomb model, and the strength is about 144 MPa when b=0. Obviously, the intermediate principal stress makes the strength increase to 150 MPa when b=1. In addition, the strength is 149 MPa when b=0.8, and the strength is 147 MPa when b=0.5. Both the theoretical and test values are listed in Table 16.4.

The comparisons between numerical modeling results based on the unified strength model and theoretically analytical results based on the unified strength theory are presented in Table 16.4. It can be found from Table 16.4 that the user-defined model, i.e., unified strength model for analysis in Flac-3D, reflects very well the characteristics of the unified strength theory.

Table 16.4 Numerical simulation and theoretically analytical results based on UST

	Principal stresses	$\sigma_2(\sigma_x)$ (MPa)	$\sigma_3(\sigma_y)$ (MPa)	$\sigma_1(\sigma_z)$ (MPa)
b=0	Theoretically analytical result	110	100	143.6
	Numerical modeling result	110	100	143.2
b=1	Theoretically analytical result	110	100	150.0
	Numerical modeling result	110	100	150.3
b=0.8	Theoretically analytical result	110	100	149.0
	Numerical modeling result	110	100	149.4
b=0.5	Theoretical analytical result	110	100	147.2
	Numerical modeling result	110	100	147.9

16.8 Stability Analysis of Underground Powerhouse

16.8.1 Generation of Numerical Model and Selection of Parameters

The size of the numerical model is 240 m × 100 m × 260 m. The main power house is 22.3 m wide and 51.3 m high. The main transformer cave is 17.9 m wide and

32.2 m high. The outer boundaries have been modeled at a distance of around six tunnel widths from the tunnel in both directions to minimize the boundary effect on the analytical results. There are 44760 zones and 28017 grids in the model, which is shown in Fig. 16.4.

The in-situ stresses are applied on the boundary surfaces. The properties for the intact rock based on the experimental data are applied to the rock mass using the Hoek-Brown criterion. The properties of some rocks and the stresses are listed in Table 16.5.

Table 16.5 Property of some models

Rock type	Unit weight ($kN/m^{3)}$	Bulk modulus (GPa)	Shear modulus (GPa)	b	α	Dilation angle (°)	Rock classes CSIR	Tensile strength (MPa)
Tuff-agglomerate	27.6	21.74	17.69	0.15	0.23	0	Good rock	1.5
Andesite-tuff	27.0	22.31	17.44	0.13	0.21	0	Good rock	0.9
Interbeds of andesite-tuff and tuff-agglomerate	27.3	21.68	17.64	0.21	0.31	0	Good rock	1.36

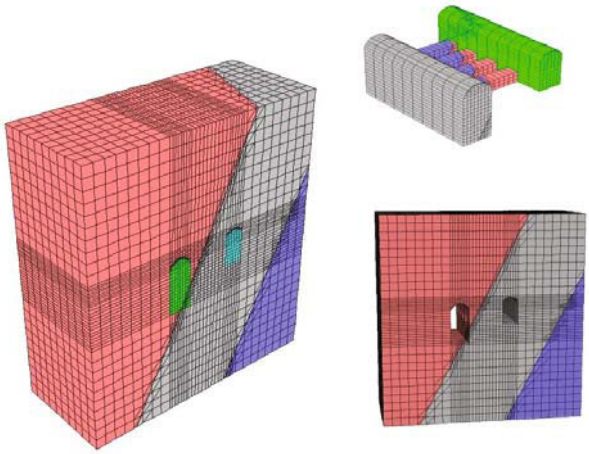

Fig. 16.4 Modeling for numerical analysis

16.8.2 Simulations for Different Excavation Schemes

The excavation of a cavern is always carried out step by step. In order to allow a reasonable step height and excavation procedures, simulations with different construction schemes are carried out. The specifications of hydraulic projects show that the step height should be about 8 m, so heights of 9 m and 12 m are

chosen in numerical modeling for the examples. There are two excavation sequences for each example with different step heights. Figures. 16.5 and 16.6 illustrate the schemes.

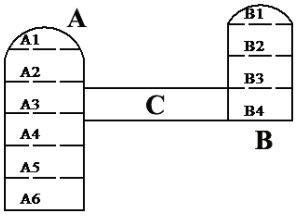

Fig. 16.6 Scheme with the step height is 12 m

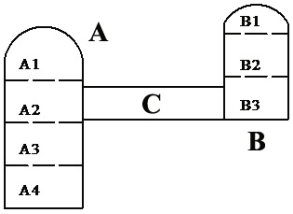

Fig. 16.5 Scheme with the step height is 9 m

The excavations cause plastic failure in certain regions. In the unified strength model, the sign shear-n shows that the zone is now in a state of shear failure, and the sign shear-p shows that the zone was previously in a state of shear failure and is elastic now. Selected results are shown in Figs. 16.7~16.11. Some researchers prioritise against displacement and a failure region by using the analytic hierarchy process method. Considering that the failure around the power house is mainly affected by the scale of the excavation and the excavation sequence makes a minor contribution, we establish the criteria for analyzing the stability of the power house based on the principles of the New Austrian Tunneling Method.

Table 16.6 Scheme of excavation procedure with 9 m height step

First sequence with step height of 9 m				Second sequence with step height of 9 m			
Excavation sequence number	Main power house	Main transformer	Omnibus bar cave	Excavation sequence number	Main power house	Main transformer	Omnibus bar cave
1	A1	B1		1	A1		
2	A2	B2		2	A2		
3	A3	B3		3	A3	B1	
4	A4	B4	C	4	A4	B2	C
5	A5			5	A5	B3	
6	A6			6	A6	B4	

Table 16.7 Scheme of excavation procedure with 12 m height step

First sequence with step height of 12 m				Second sequence with step height of 12 m			
Excavation sequence number	Main power house	Main transformer	Omnibus bar cave	Excavation sequence number	Main power house	Main transformer	Omnibus bar cave
1	A1	B1		1	A1		
2	A2	B2		2	A2	B1	
3	A3	B3	C	3	A3	B2	C
4	A4			4	A4	B3	

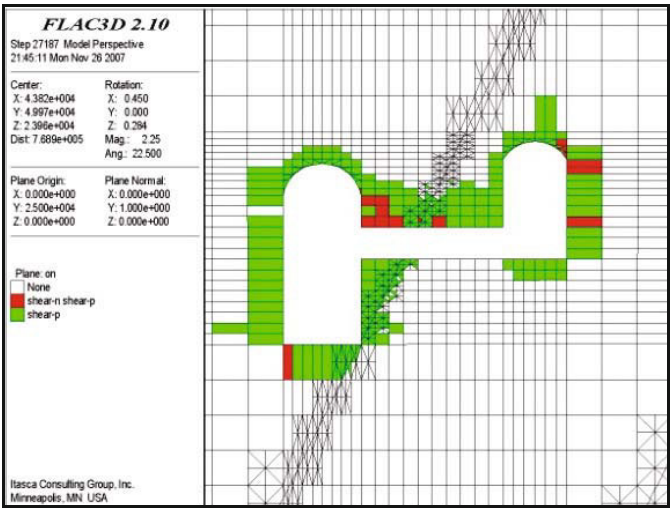

Fig. 16.7 Distributions of failure zones at last step in the first excavation sequence of the scheme

Distributions of failure zones in the first excavation sequence of the scheme are shown in Fig. 16.7 and Fig. 16.8. The step height is 9 m. Figure 16.7 shows the distributions of failure zones at the last step in the first excavation sequence of the scheme. Other failure zones at different steps are shown in Fig. 16.8. Distributions of failure zones in the second excavation sequence of the scheme are shown in Fig. 16.9. The step height is also 9 m.

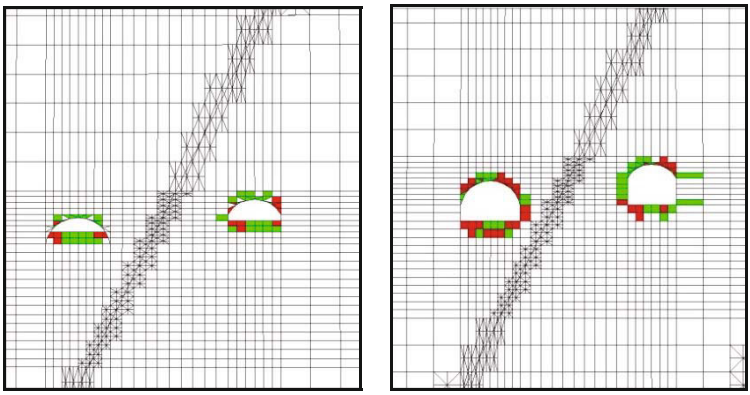

(a) First step (b) Second step

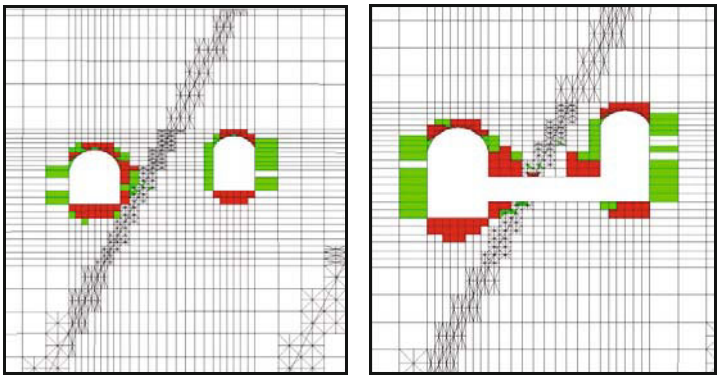

(c) Third step (d) Fourth step

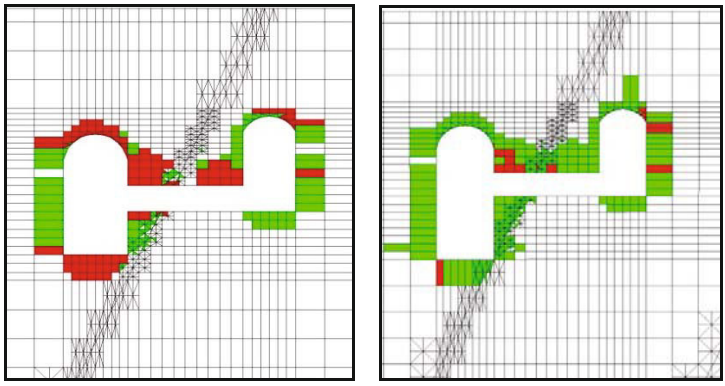

(f) Fifth step (g) Sixth step

Fig. 16.8 Distributions of failure zones in the first excavation sequence of the scheme

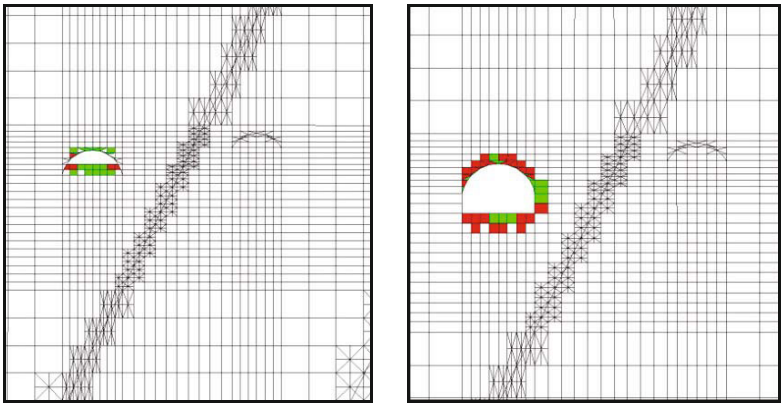

(a) First step (b) Second step

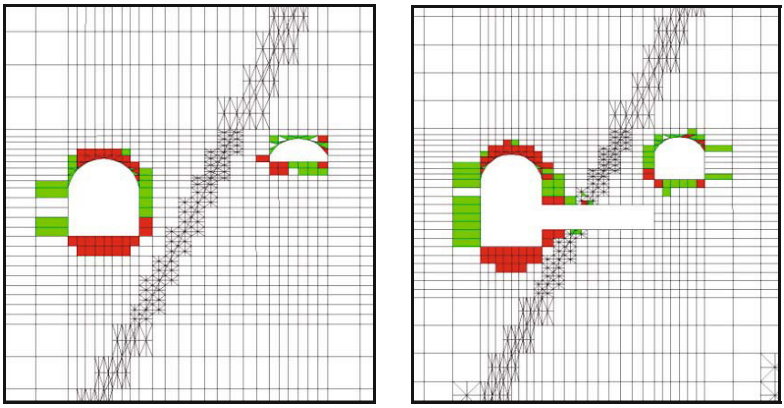

(c) Third step (d) Fourth step

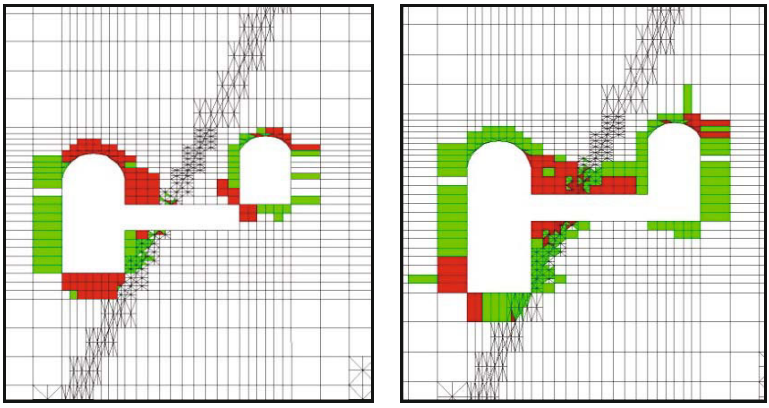

(e) Fifth step (f) Sixth step

Fig. 16.9 Distributions of failure zones in the second excavation sequence of the scheme with the step height is 9 m

Distributions of failure zones in the first excavation sequence of the scheme are shown in Fig.16. 10. The step height is 12 m. Distributions of failure zones in the second excavation sequence of the scheme are shown in Fig. 16.11. The step height is also 12 m

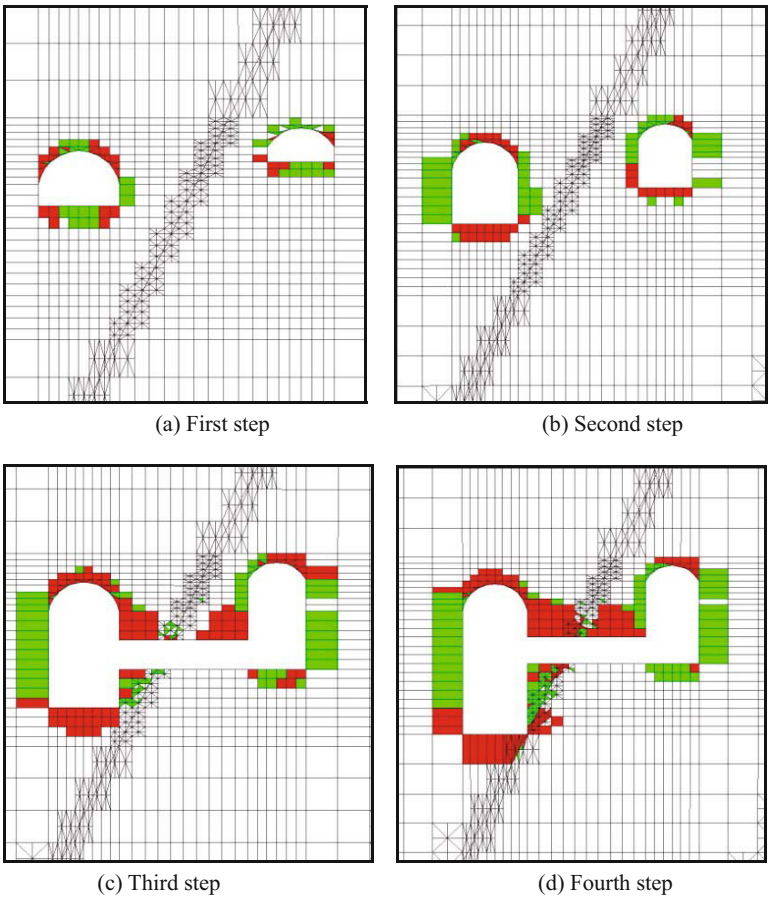

(a) First step (b) Second step

(c) Third step (d) Fourth step

Fig. 16.10 Distributions of failure zones in the first excavation sequence of the scheme with the step height 12 m.

The New Austrian Tunneling Method (NATM) is very important for the design of tunnels. The method complies with the principles of measuring frequently, supporting in time, and closing the steel arch early. To choose a reasonable excavation procedure, which will have the minimum impact on the rock mass and where the reinforcement of the tunnel can be supported relatively earlier, a comparison of four excavation procedures is carried out. Each of the four schemes reveals the following features:

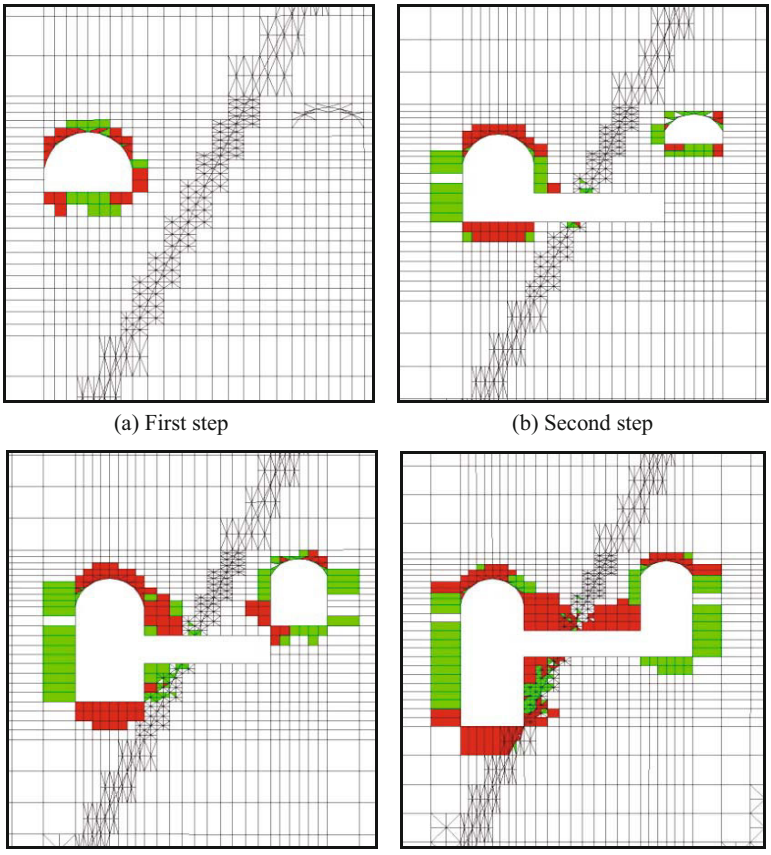

(a) First step (b) Second step

(c) Third step (d) Fourth step

Fig. 16.11 Distributions of failure zones in the second excavation sequence of the scheme with the step height 12 m

(a) The failure region on the top of the tunnel is small, but the larger the excavation scale, the larger is the extent of the failure region.

(b) Plastic regions can be very close to each other because of the excavation of the main power house tunnel and the main transformer cave (i.e., cavern A and cavern B in Figs. 16.5 and 16.6)

(c) Omnibus bar caves (i.e., cave C in Figs. 16.5 and 16.6) excavated in the rock masses within the plastic zones are very unstable.

(d) Excavation of omnibus bar caves causes a secondary disturbance to the failure regions of the walls between the main power house tunnel and the main transformer cave.

To minimize the impact of the excavation of omnibus bar caves (i.e., cave C in Figs. 16.5 and 16.6) on the failed rock mass, to finish the excavation and the support of omnibus bar caves earlier, and to decrease the extent of the plastic region caused by the excavation of the first step, the first excavation

sequence with a 9 m height step is selected as the excavation scheme, which is subsequently used for the following supporting analysis.

16.9 Excavation and Support Modeling

The first excavation sequence with a 9 m height step is chosen for the following supporting analysis. First, supports for the initial design are given.

Supports for the main power tunnel and the main transformer caverns:

Length of the fully grouted rebar bolt installed in top rock	5 m
Length of the fully grouted rebar bolt installed in wall	4.5 m
Rebar diameter	32 mm
Rebar bolting pattern	1.5 m×1.5 m
Length of the cable installed in wal	20 m
Cable bolting pattern	4.5 m×6 m
Tensile strength of cable	2×10^5 kg

Supports of omnibus bar caves:

Length of the fully grouted rebar bolt	4 m
Rebar bolt diameter	28 mm
Rebar bolting pattern	3 m×3 m
Shotcrete type Chinese C20	
Liner thickness	15 cm

The supports are illustrated in Fig. 16.12.

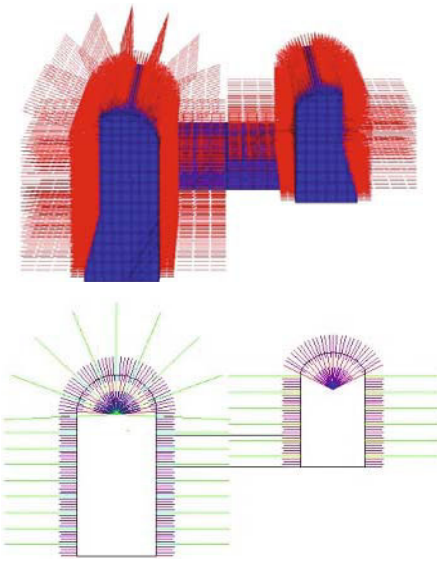

Fig. 16.12 Supports of the caverns

After a balance is reached, selected results are shown in Figs. 16.11~6.14. Distribution of the failure regions on a vertical plane is shown in Fig. 16.13. The contour of vertical displacements along the *z*-axis is shown in Fig. 16.14 and the contour of the horizontal displacement is plotted in Fig. 16.15.

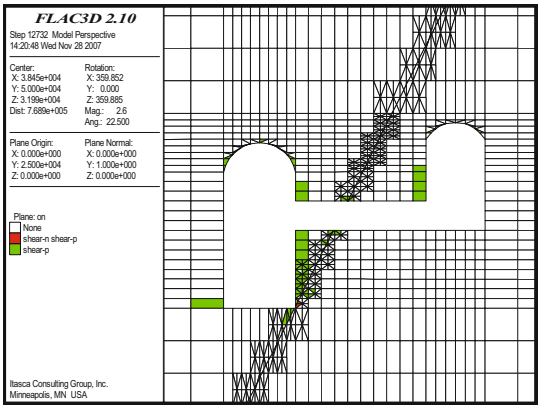

Fig. 16.13 Plastic region distribution with the support in initial design

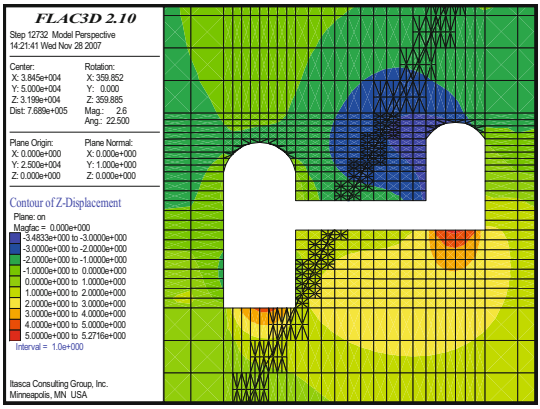

Fig. 16.14 Contour of virtical displacement with the support in initial design.

It is obvious that the tunnel is stable, the plastic zones can only be found in the wall and the extent is small. The maximum subsidence of the tunnel roof is 4 mm and the maximum vertical displacement of the main transformer cavern is located on the side and close to the main power-house. The maximum convergence in a horizontal direction is about 28 mm.

Considering that the support stiffness is high in this case, we adjusted the parameters of the support as follows:

(a) Took off the cables anchored at the top of the main power house in the initial design.

(b) Transferred the pattern of rebar bolting to 2 m×2 m.

The modeling results are shown in Figs. 16.16~16.18.

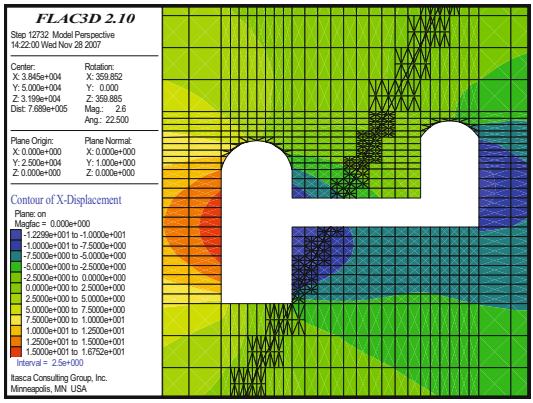

Fig. 16.15 Contour of horizontal displacement in the second design

When the stiffness of the support is degraded, the plastic region is beyond the range covered by the rebar bolts. The maximum subsidence of the tunnel roof is 7.8 mm and the maximum convergence is 55 mm. It can be seen that the support stiffness of the side walls of the main power-house tunnel in the second design is not enough, so a rebar bolt pattern of 1.5 m×1.5 m should be selected for the support of the main power-house tunnel side walls.

During the construction, the measurements based on the principles of reasonable engineering should be applied and the pattern should be tailored, on site, to the idiosyncrasy of the project. From the analysis above, the values of parameter b are both 0.33.

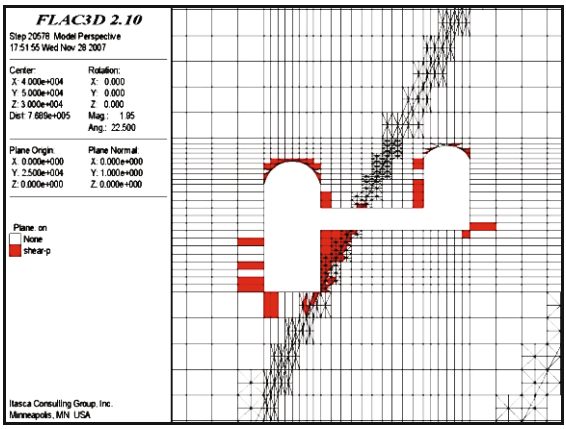

Fig. 16.16 Plastic region distribution with the support

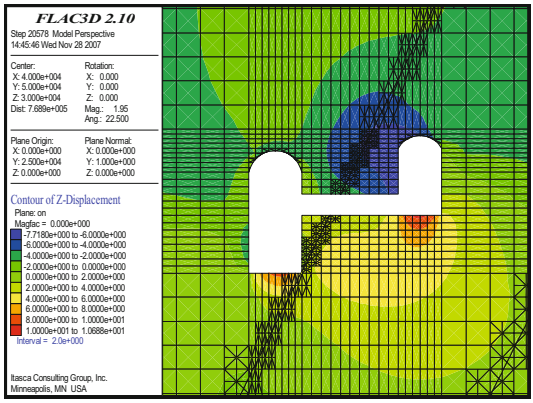

Fig. 16.17 Contour of virtical displacement with the support in second design

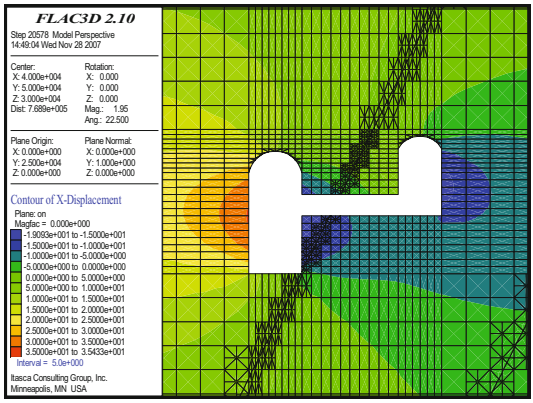

Fig. 16.18 Contour of horizontal displacement in the support second design.

16.10 Comparison of the Stabilities in these Models with Different *b* Values

The selection of different values of parameter b in the unified strength theory can provide a series of failure criteria, such as the single-shear (Mohr-Coulomb) yield criterion (when b=0) and twin-shear yield criterion (when b=1). Because of the variety of strength envelopes of unified strength theory on the π plane, different strength values can be obtained in the same stress state. An engineer should make a reasonable design to find which one is appropriate for the engineering objective, and which strength criterion of rock masses is the most contributing factor affecting our designs. None of the failure criteria can universally be utilized in overall rock masses, so we can compare the results obtained from different constitutive models with the same geometry, the same properties but with different

values of parameter b. The support in the second design is installed, and the results are illustrated in Figs. 16.19, 16.20 and 16.21, which show the variety of plastic region, vertical displacement and horizontal displacement of the models with different values of parameter b in the second support design

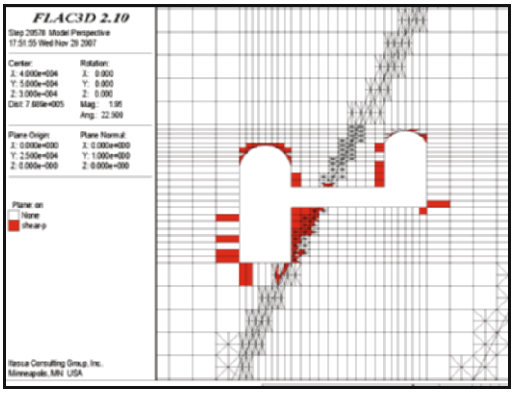

(a) UST with b=0.3

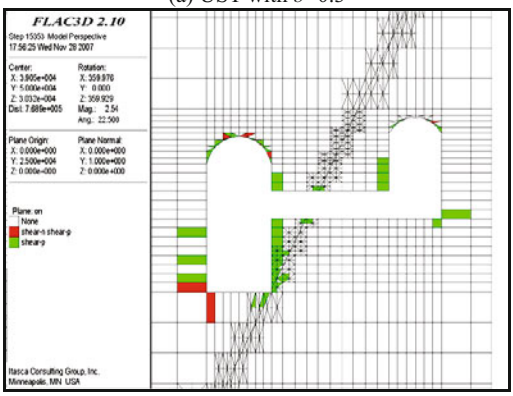

(b) UST with b=0.5

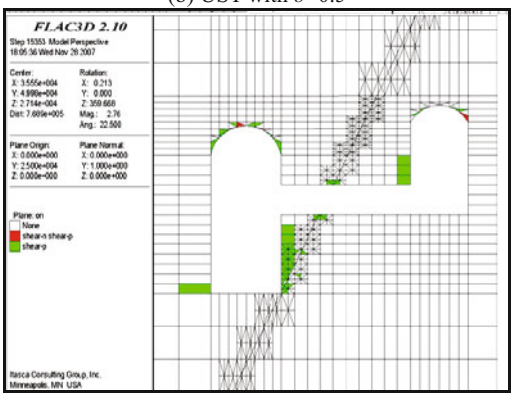

(c) UST with b=0.8

Fig. 16.19 Variety of plastic region of the models with different values of parameter b

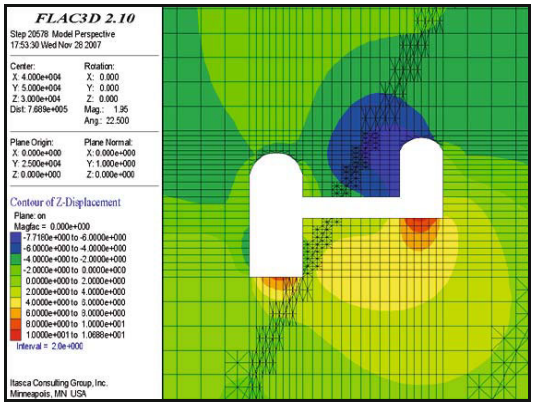

(a) UST with b=0.3

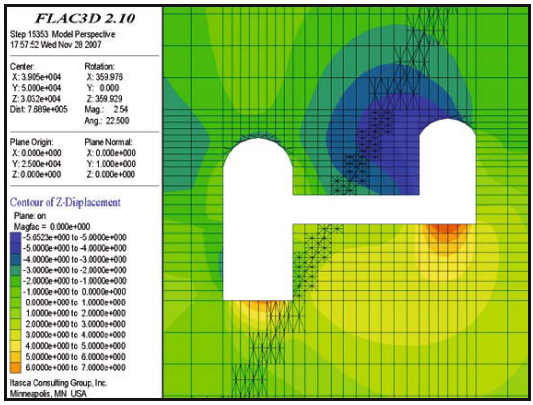

(b) UST with b=0.5

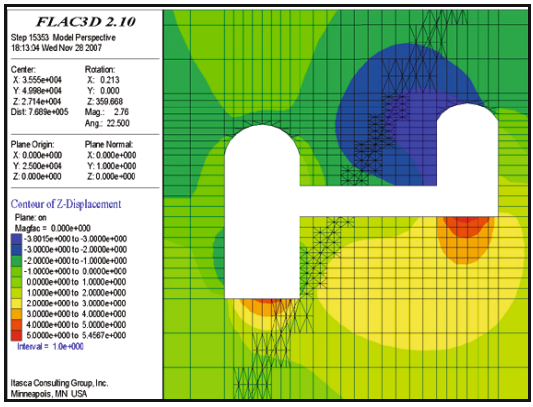

(c) UST with b=0.8

Fig. 16.20 Variety of vertical displacement of models with different parameter b

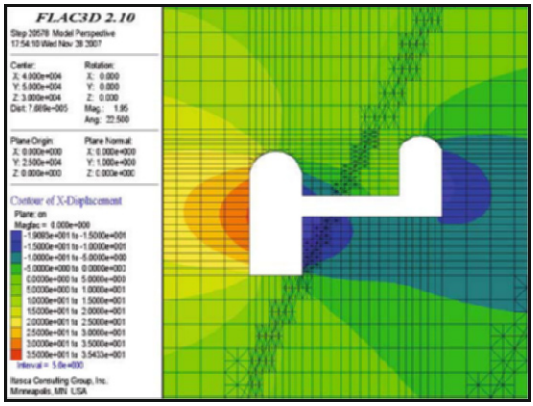

(a) UST with b=0.3

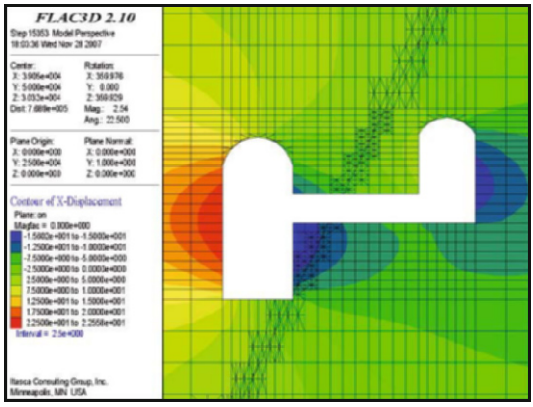

(b) UST with b=0.5

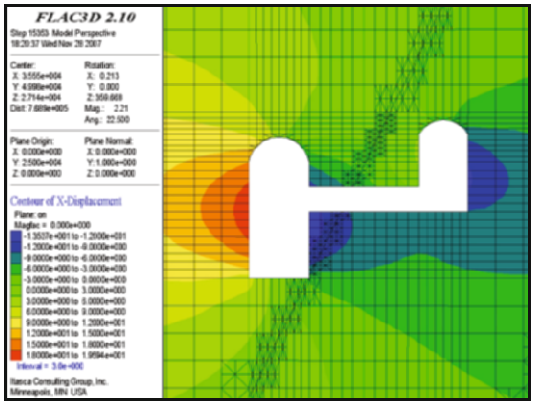

(c) UST with b=0.8

Fig. 16.21 Variety of horizontal displacement of models with different parameter b

It can be seen that the effect of the intermediate principal stress is incorporated in numerical modeling by the parameter b in unified strength theory, which affects the distribution of failure zones and the contour of displacements. The spread of the plastic region of the main transformer cavern and the main power-house becomes smaller when the value of parameter b increases from 0.3 to 0.5. The maximum roof subsidence is 5.6 mm when b=0.8. The parameters of support and the mechanical properties of the rock mass are the same but the range of the plastic region and the displacements of grids are all similar to those with the same support as in the initial design. In the construction of a hydraulic project, high values of stiffness and strength are usually accepted, so the stabilization results from numerical modeling with different strength criteria may be similar. But enormous economic benefits might be obtained in the construction of projects if a large plastic region is allowed.

16.11 Conclusions

Compared to the popular strength criteria used for geomaterials, the unified strength theory is selected for the stability analysis of the power station. Considering the absence of the unified strength model in Flac-3D constitutive models, a unified strength model with a non-associated flow rule is developed using the C++ language. True triaxial simulation tests are implemented, and the stress-strain curves based on the Mohr-Coulomb model and the unified strength model are obtained, respectively. According to the comparison with the simulation results, the unified strength model can reasonably represent the effect of the intermediate principal stress.

Through the numerical stability analysis of Huanren pumped storage power station using the unified strength theory, the following conclusions are made:

(a) Because of the large scale of excavation, the rock mass between the main power-house tunnel and the main transformer tunnel will fail seriously if a support system is not installed. In this case, the maximum horizontal principal stress normal to the tunnel axis is harmful to the stability of the caverns. So the principles of the New Austria Tunneling Method should be followed and the excavation of the rock mass in the tunnel roof should be carried out in small steps in order to reduce the range of failure. According to the analysis of results from the numerical modeling of unsupported tunnels, a first excavation sequence is proposed.

(b) It can be obtained from the calculated results using the unified strength model inserted in Flac-3D that the support stiffness in the initial design is high. Hence, some substitutions of the support parameters are used for further analysis. The results from the second support design show that the range of the plastic region in the tunnel side walls becomes larger, the maximum subsidence of the tunnel roof goes from from 4 mm to 7.8 mm, and the maximum convergence goes from 28 mm to 55 mm.

(c) The different values of parameter b make failure conditions of the caverns vary within a certain range. In this case, the stable state obtained from b=0.3 in the initial design is similar to that obtained from b=0.8 in the second design. It is shown that estimation and determination of the intermediate principal stress is important for the stability analysis and can have an important effect on the financial benefit.

References

Li XC and Xu DJ (1990) Experimental verification of the twin shear strength theory–true triaxial test research of strength of the granite in a large power station on Yellow River. Research Report (Rock and Soil 1990-52) of Institute of Rock and Soil Mechanics. Chinese Academy of Sciences (in Chinese).

Li Y (2008) In-situ Stress Measurement and Stability Analysis Based on the Unified Strength Theory in Large Scale Underground Caverns Zone. Doctoral Dissertation, Beijing Scientific and Technical University.

Mogi K (1967a) Effect of the intermediate principal stress on rock failure. J. Geophysics Res., 72: 5117-5131.

Mogi K (1967b) Effect of the triaxial stress system on fracture and flow of rock. Phys. Earth Planet Inter., 5: 318-324.

Mogi K (1979) Flow and fracture of rocks under general triaxial compression. Proc. of 4th Int. Congress on Rock Mechanics (Montreux), Balkema, Rotterdam, Vol: 123-130.

Xu DJ and Geng NG (1984) Rock rupture and earthquake caused by change in the intermediate principal stress. Acta Seismologica Sinica, 6(2): 159-166 (in Chinese).

Xu DJ and Geng NG (1985) The variation law of rock strength with increase in intermediate principal stress. Acta Mechanics Solida Sinica, 7: 72-80 (in Chinese, English abstract).

Yu MH (1961a) General behavior of isotropic yield function. Research Report of Xi'an Jiaotong University. Xi'an, China (in Chinese).

Yu MH (1961b) Plastic potential and flow rules associated singular yield criterion. Research Report of Xi'an Jiaotong University. Xi'an, China (in Chinese).

Yu MH, He LN and Song LY (1985) Twin shear stress theory and its generalization. Scientia Sinica (Sciences in China), English edn. Series A, 28(11): 1174-1183.

Yu MH (1998) Twin Shear Theory and its Applications. Science Press: Beijing (in Chinese).

Yu MH (2004) Unified Strength Theory and its Applications. Springer: Berlin.